

Showcasing research from Cornell University, Ithaca, USA.

Block copolymer derived 3-D interpenetrating multifunctional gyroidal nanohybrids for electrical energy storage

A lithium ion battery with an ordered three-dimensional (3-D) architecture ("3-D battery") is synthesized from block copolymer self-assembly in a core-shell double gyroid structure. Rather than using a conventional layered approach, this architecture folds carbon anode, polymer electrolyte, and sulfur cathode into an interpenetrating co-continuous nanonetwork with separation lengths of less than 20 nm between the electrode networks. The gyroidal nanostructure decreases the lithium ion diffusion length to tens of nanometers within an overall macroscopic electrical energy storage device.

As featured in: Energy & Environmental Science See U. Wiesner et al., Energy Environ. Sci., 2018, 11, 1261.



Energy & Environmental Science



View Article Online PAPER



Cite this: Energy Environ. Sci., 2018. 11. 1261

Block copolymer derived 3-D interpenetrating multifunctional gyroidal nanohybrids for electrical energy storage†

J. G. Werner, oab G. G. Rodríguez-Calero, H. D. Abruña band U. Wiesner *

Electrical energy storage systems such as batteries would benefit enormously from integrating all device components in three-dimensional (3-D) architectures on the nanoscale to improve their power capability without negatively impacting the device-scale energy density. However, the lack of large scale synthesis methods of 3-D architectures with precise spatial control of multiple, functional energy materials at the nanoscale remains a key issue holding back the development of such intricate device designs. To achieve fully integrated, multi-material nano-3-D architectures, next-generation nanofabrication requires departure from the traditional top-down patterning methods. Here, we present an approach to such systems based on the bottom-up synthesis of co-continuous nanohybrids with all necessary functional battery components rationally integrated in a triblock terpolymer derived core-shell double gyroid architecture. In our design three-dimensional periodically ordered, functional anode and cathode nanonetworks are separated by an ultrathin electrolyte phase within a single 3-D nanostructure. All materials are less than 20 nm in their layer dimensions, co-continuous and interpenetrating in 3-D, and extended throughout a macroscopic monolith. The electrochemical analysis of our solid-state nano-3-D Li-ion/sulfur system demonstrated batterylike characteristics with stable open circuit voltage, reversible discharge voltage and capacity, and orders of magnitude decreases in footprint area compared to two-dimensional thin layer designs.

Received 18th December 2017 Accepted 8th March 2018

DOI: 10.1039/c7ee03571c

rsc.li/ees

Broader context

Advances in energy storage will have a growing impact on society with the expansion of portable electronics, and for the future of electric mobility and renewable but intermittent energy sources. Apart from increasing the amount of stored energy, the speed with which energy can be released or stored is a crucial parameter. This socalled power density of batteries is significantly increased when using nanostructured electrodes that provide fast ion transport and reaction kinetics. Such architectures, however, still typically have the anode and cathode separated over macroscopic length scales. Therefore, merely nanosizing electrodes increases their porosity and causes a decrease in the amount of energy that a device can store. In contrast, in this work, we fold nanoscopic cathode and electrolyte/separator layers into the nanopores of a monolithic and three-dimensionally continuous anode nanonetwork, removing their macroscopic separation. This enables the most efficient utilization of space, not wasting device volume or mass to excess electrolyte. While this approach has been conceptualized over 15 years ago, translation into a successfully operating device with all dimensions below 50 nm has remained elusive due to the incredible complexity of the necessary multifunctional nanostructure and strict material requirements. This work demonstrates that successful and reversible battery characteristics can be obtained with such nanoscale structures, with orders of magnitude smaller dimensions than used in common composite or even thin-film batteries.

Introduction

Miniaturization of device components in electronics has brought around the technological revolution of the past decades.¹

The tremendous research and development in top-down microand nanofabrication has enabled the constant decrease of feature sizes, increasing the density of transistors and with that the capability of modern electronic devices.2 This technological advancement was made possible by material innovations in high-resolution lithographic patterning and deposition techniques.3,4 Standard nanofabrication processes use twodimensional (2-D) top-down patterning to transfer designs into multiple functional materials that are deposited layer by layer. 4 The next step in multi-material device design is the utilization of three-dimensional (3-D) continuous architectures with nanometric features instead of planar 2-D stacks.⁵ The use of the

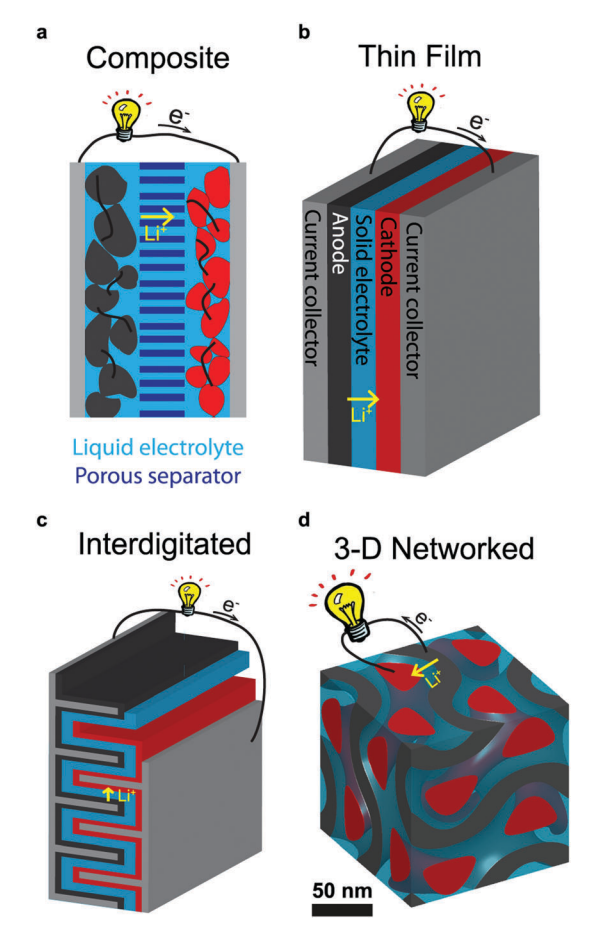
^a Department of Materials Science and Engineering, Cornell University, Ithaca, NY 14853, USA. E-mail: ubw1@cornell.edu

^b Department of Chemistry and Chemical Biology, Cornell University, Ithaca, NY 14853, USA

[†] Electronic supplementary information (ESI) available: Detailed experimental procedures, material characteristics, additional SEM images, small-angle X-ray scattering and nitrogen sorption data, and galvanostatic and potentiostatic electrochemical data. See DOI: 10.1039/c7ee03571c

third dimension in device architectures is particularly crucial if high interfacial areas or high material loading per footprint area of the device are beneficial.⁶⁻⁸ While developments in top-down photolithographic techniques and materials have enabled large-scale access to ever decreasing feature sizes in 2-D architectures, the fabrication of nanosized 3-D features suffers from slow and expensive processes. Some top-down technologies enable precise structural control in three dimensions on the nanoscale, such as two-photon lithography, but they are mostly inapplicable to large scale manufacturing. 9 Bottom-up selfassembly is considered a viable and cost-effective path to overcome many of the existing limitations in 3-D nanofabrication. The nature of self-assembly enables the production of nanostructures at large scales without time-consuming and scale-limiting steps of active nanomanipulation. 10,11

Electrical energy storage (EES) devices such as batteries would benefit tremendously from 3-D integrated architectures. 12,13 While the physical properties of materials such as (semi)conductivity define their performance in electronics, EES devices such as batteries are characterized by the amount of energy that is stored and its accessibility. This poses additional challenges associated with chemical reactions and transportation of ionic materials integral to device function. In batteries, energy is stored through chemical redox reactions of ions in separate anode and cathode materials, between which the ions shuttle during charge and discharge.14 The amount of energy stored is proportional to the amount of active anode and cathode material, as well as their storage capacity per mass or volume. The achievable power of a battery depends on how fast this energy is accessible, which in most commonly employed EES systems is limited by the diffusion and reaction of ions in the solid electrode materials. Batteries with nanostructured architectures promise improved power output, as close proximity of the two electrodes is beneficial for fast ion diffusion, while high material loading simultaneously enables high energy density. 12 However, in the past, improvement of one has often had a negative impact on the other. 15-18 Since ionic diffusion is orders of magnitude faster in liquids than in solids, most lithium ion batteries employ a liquid electrolyte infused porous membrane for ionic transport between composite electrodes (Scheme 1a).14 A widely employed strategy over the past two decades to increase the power capabilities of batteries with faster charge and discharge is based on decreasing the active feature sizes of the materials and increasing their porosity, in order to decrease solid state diffusion distances. 19-22 While this tremendously improves power capabilities, it simultaneously decreases the amount of active material per volume and area, and hence the overall energy density of the device. 15 Thin film batteries overcome this issue by using micrometer thin stacks of anode-electrolyte-cathode layers, commonly employing solid electrolytes (Scheme 1b).²³ The thinner the films, the shorter the ion diffusion distances yielding higher power densities, but at the same time decreasing the amount of material and energy stored. By employing the third dimension, short distances of all components can be maintained for fast ion transport while increasing the amount of charge-storing



Scheme 1 Illustration of different battery architectures: commonly employed composite (a), thin film (b), interdigitated thin film (c), and 3-D gyroidal (d) designs.

material per footprint area. This has been achieved by using interdigitated designs of 1- and 2-D electrodes, but mostly with micron-scale feature sizes (Scheme 1c). 24-26 Such interdigitated architectures also lack structural stability, especially when nanoscale dimensions are approached.²⁷ Continuous networks of anode, electrolyte, and cathode folded in 3-D would improve structural integrity while providing all the beneficial properties of short ion-diffusion distances and 3-D connectivity for electron transport (Scheme 1d).12 In such 3-D EES architectures, energy and power densities on the device scale are decoupled from each other, depending independently on the storage capacity and separation length-scale of the materials, respectively. 12,13

While the concept of 3-D nano-networked architectures for EES systems offers tremendous advantages over conventional designs, 12 only very few reports of such systems with nanoscale dimensions exist and a working device remains elusive. ^{28,29} The challenges to fabricate the functional materials necessary for a battery in a 3-D continuous nano-architecture are immense. Strict separation of anode from cathode networks throughout the entire nanostructure is required to avoid short circuits which would render the entire device inoperable. The electrode phases have to be redox active and electronically conductive at the same time, while the electrolyte has to provide ionic

conductivity while inhibiting electronic contact between the interpenetrating anode and cathode. Incorporating such functional materials and components into a 3-D continuous nanoarchitecture imposes tremendous processing challenges, and even highly precise deposition techniques such as atomic layer deposition (ALD) to date are inapplicable.30

Here, we describe a bottom-up fabrication method that enables the spatially precise synthesis of all necessary functional battery materials folded into a 3-D periodically ordered core-shell double gyroidal morphology with phase dimensions of below 20 nm, and report their first successful proof-ofconcept application as an EES system. The core-shell double gyroid is a three-dimensional network morphology that exhibits all the structural requirements discussed above (Scheme 1d),³¹ and can be found in a number of self-assembling systems such as block copolymers, lipids, and microemulsions, and occurs in nature as the basis of structural color in butterfly wings. 32-35 It is described by Schoen's G minimal surface that separates the space into two interpenetrating 3-D continuous volumes with opposite chirality.³⁶ In triblock terpolymer-derived core-shell double gyroids (G^D), this surface splits laterally, defining a third continuous matrix volume (gray in Scheme 1d) that separates two core-shell networks (red core and blue shell domains in Scheme 1d) with strut dimensions on the order of tens of nanometers.³⁷ The matrix phase is completely separated from the two core network phases by two shell phases, resembling the ideal case of a 3-D anode-electrolyte-cathode architecture and providing a plausible path towards nano-3-D batteries (Fig. 1a). Despite inefficiencies in their performance expected at this early point, the measured capacities of the gyroidal 3-D nano-scaled batteries reported here were three orders of magnitude higher when compared to those of a theoretical flat (2-D) architecture with the same nanoscale dimensions and footprint area. and 45 times higher than the only previously claimed successful prototype of a 3-D EES architecture with all-nanoscale features.²⁸

Results and discussion

Gyroidal mesoporous carbon (GDMC) monoliths as a simultaneous anode active material and current collector

Our nano-3-D battery concept employs the core-shell double gyroid morphology to fold anode, electrolyte, and cathode into a 3-D continuous nanostructure. Homogeneity, mechanical properties, and transport characteristics make the gyroidal morphology a promising candidate for the synthesis and exploration of fully nano-integrated 3-D EES devices. 38,39 While certain triblock terpolymers spontaneously self-assemble into a core-shell double gyroid morphology, polymers with blocks exhibiting anode, electrolyte, and cathode properties are unheard of. We therefore employed a

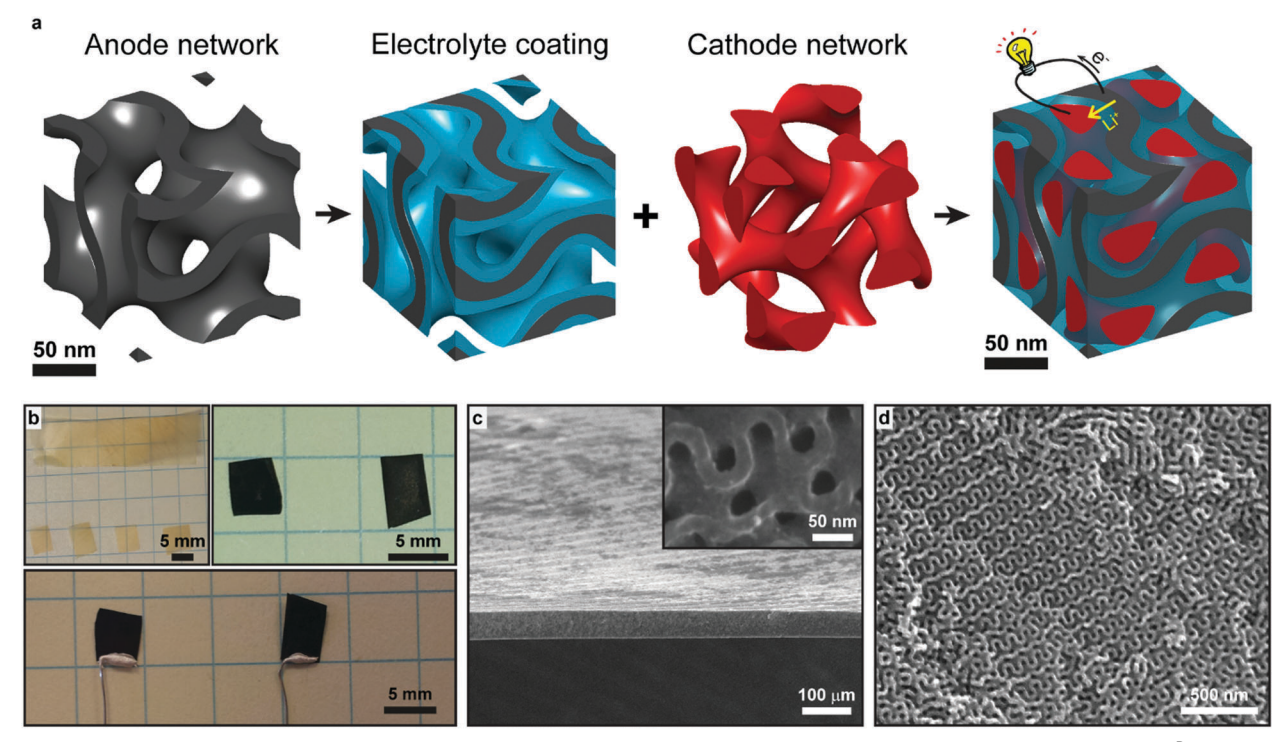


Fig. 1 Assembly of a penta-continuous interpenetrating and nanostructured hybrid from double gyroidal mesoporous carbon (GDMC) monoliths. (a) Schematic illustration of the synthesis pathway: a redox-active and conductive carbon anode with gyroidal 3-D structure (GDMC) and finite wall thickness (black) is conformally coated with nanoscaled polymer electrolyte (blue), here poly(phenylene oxide). The remaining two interpenetrating network mesopore channels are back-filled with a redox-active and conductive cathode (red), here a composite of sulfur and poly(3,4ethylenedioxythiophene), respectively. (b) Photographs of the as-made BCP-organic hybrids (top left), GDMC monoliths after carbonization (top right), and $G^{D}MC$ monoliths electrically contacted in the edge-on geometry (bottom). (c and d) SEM images of a $G^{D}MC$ monolith exhibiting uniform thickness (c), surfaces with open and accessible gyroidal mesoporosity (c, inset), and uniform gyroidal cross-section (d).

gyroidal mesoporous anode framework and synthesized the remaining functional battery components confined within its porous nanonetworks in a step-wise bottom-up approach (Fig. 1a). The anode framework has to fulfill numerous requirements, including lithium redox chemistry at low potentials, electrical conductivity, structural integrity, and large, homogeneously connected mesopores to allow enough space for the subsequent nanoconfined electrolyte and cathode depositions. Gyroidal mesoporous carbon (GDMC) monoliths recently developed matched these properties well and were chosen as the anode framework.40 GDMC materials were synthesized through self-assembly of a large molar mass triblock terpolymer (130 kDa, Table S1, ESI†), poly(isoprene)-block-poly(styrene)block-poly(ethylene oxide) (ISO), in the presence of oligomeric phenol-formaldehyde resols as carbon precursors vielding a polymer-organic hybrid with the core-shell double gyroid morphology. Pyrolysis of the hybrids led to degradation of the block copolymer and carbonization of the resols, resulting in electrically conductive, ordered 3-D gyroidal carbon networks with large, homogeneous mesopores of 40 nm in diameter, porosity of 63 vol%, and a carbon wall thickness of 15 nm (Fig. 1b-d, Fig. S1 and Table S2, ESI†). Comprehensive synthesis and characterization details of these carbons are described elsewhere. 40 The facile casting procedure to fabricate the coreshell double gyroid hybrids is inherently compatible with standard polymer processing and enables the formation of macroscopic

monoliths of fairly arbitrary size and shape (Fig. 1b). The freestanding monolithic GDMCs used here had a homogeneous thickness chosen to be approximately 70 microns and accessible mesoporosity from all surfaces (Fig. 1c and d). The geometry led to an average carbon area density of 5 mg cm⁻², although the thickness is tunable to obtain a desired areal carbon loading. The homogeneous morphology of the gyroid networks ensured good accessibility for the subsequent synthesis steps, a key requirement for the step-wise nanoconfined synthesis of all EES components. Inhomogeneous porosity as found in aerogels or inverse opal structures exhibits bottle necks that can prove detrimental for nanoconfined depositions. The gyroidal mesoporous carbon material was evaluated as an anode material in a standard coin cell test, which confirmed the carbon-lithium redox activity with a reversible capacity of 220 mA h g^{-1} (Fig. S2, ESI†). Freestanding G^DMC monoliths were wire-contacted (Fig. 1b), rendering the entire gyroidal carbon network electrochemically accessible for the subsequent surface-confined polymer electrolyte synthesis, and served as the anode contact of the final nano-3-D EES device.

Conformal ultrathin solid electrolyte/separator coating

The electrolyte has to ensure electronic insulation, but allow ionic transport, between the cathode and anode networks. Any pinholes that cause contacting of the two interpenetrating electrodes within the 3-D nanostructure would result in a short circuit and render the architecture inoperable as an energy

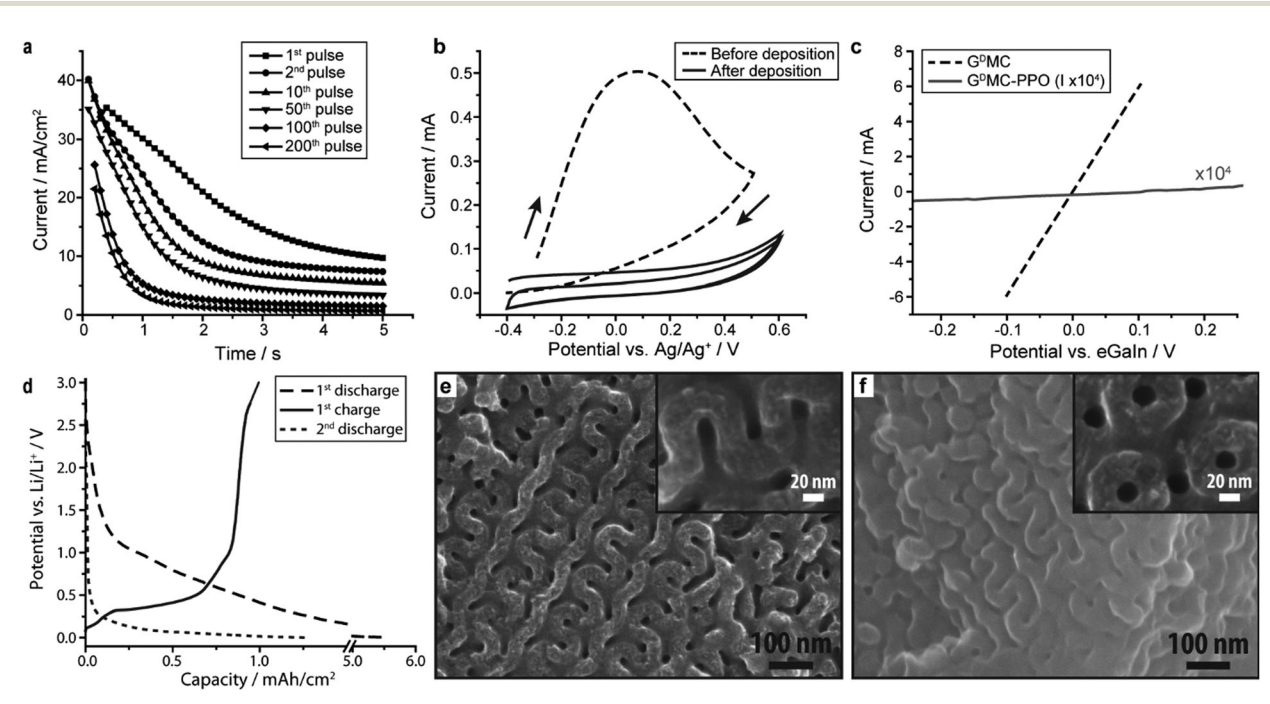


Fig. 2 Electropolymerization of the ultrathin solid polymer electrolyte on a monolithic mesoporous G^DMC anode. (a) Current–time traces of selected potentiostatic PPO electrodeposition pulses at +0.6 V vs. Ag/Ag⁺. (b) CVs of PPO-coated G^DMC electrodes in phenolate solution before and after pulsed electropolymerization exhibiting oxidation and purely double layer characteristics, respectively. (c) Two-electrode linear voltage sweep resistance measurements of the wire-connected GDMC before (dashed black) and after (solid grey) PPO electropolymerization exhibiting an increase in resistance of more than 5 orders of magnitude. Note that the current of the PPO coated GDMC was multiplied by a factor of 10⁴ to facilitate comparison. (d) Discharge and charge curves of PPO-coated G^DMC at a current of 0.1 mA cm⁻² (corresponding to approximately 20 mA g_C^{-1}), demonstrating reversible lithiation-delithiation through the PPO-layer. (e and f) SEM images of the GDMC anode after pulsed potentiostatic electropolymerization of PPO. Freshly cleaved cross-sections are depicted in (e), the monolith surface in (f), and high-magnification images in the insets.

storage device. Additionally, the electrolyte layer must not block the gyroidal mesopores to enable the subsequent deposition of the cathode phase. Coating of macroscopic 3-D nanoporous materials with conformal nanometric layers poses significant challenges to most commonly employed deposition techniques, including ALD.³⁰ Electropolymerization of insulating polymers enables self-regulating conformal growth until the entire electrochemically accessible surface is homogeneously covered, due to the propensity of deposition on previously uncoated areas (the current density on uncoated areas is much larger than on coated ones).41 Here, the GDMC anode monoliths were conformally coated with an ultra-thin solid polymer electrolyte layer, poly(phenylene oxide) (PPO), of less than 10 nm in thickness using self-limiting electropolymerization of phenol (Fig. 2). PPO had previously been shown in 2-D substrates to have the capability for forming pinhole-free, ultrathin ion-conducting yet electronically insulating layers, with selective molecular permeability tunable through the synthesis conditions. 42 In order to afford homogenous PPO thin films on the continuous gyroidal carbon surfaces, we used pulsed potentiostatic electropolymerization at +0.6 V vs. Ag/Ag⁺. During deposition, the oxidation current decayed substantially with increasing number of pulses, while the double layer current remained with attenuation (Fig. 2a). Subsequent cyclic voltammograms of PPO coated GDMCs in phenol solution showed no oxidation peak, demonstrating the electrochemical insulation of the entire accessible gyroidal carbon surface (Fig. 2b). The resulting bifunctional monoliths (anode + solid electrolyte) were extensively characterized with scanning electron microscopy (SEM), confirming the deposition of thin films throughout the G^DMC monoliths (Fig. 2e, f and Fig. S3d, ESI†). The PPO film thickness was around 8-10 nm, estimated from the wall-to-wall distance (SEM) before and after electropolymerization, with remaining 3-D continuous mesopores of 16-18 nm in size. The insulating, ultra-thin PPO polymer electrolyte layer was further evaluated using two-probe resistance and lithiation measurements. An increase in resistance of more than 5 orders of magnitude, following PPO deposition, was measured via liquid metal surface contacts (Fig. 2c). Reversible lithiation/ delithiation of PPO coated GDMCs was achieved in twoelectrode liquid cells against lithium metal, demonstrating the known permeability of the PPO layer to lithium ions and the retained carbon redox activity in our gyroidal core-shell nanoarchitecture (Fig. 2d and Fig. S2, ESI†). The observed reversible charge capacity of the PPO-coated monolithic gyroidal carbon anode was 1 mA h cm⁻² or 200 mA h g⁻¹. This was in good agreement with the reversible capacity obtained from the G^DMC material without a PPO coating in a standard coin cell test (Fig. S2a and b, ESI†). The outer monolith surfaces remained porous after PPO polymerization, maintaining accessibility of the inner mesoporosity (Fig. 2f), critical for sub-

Bifunctional cathode composite infiltration

sequent nanoconfined cathode synthesis steps.

The remaining 3-D continuous porosity in the anode-electrolyte core-shell gyroidal monoliths was utilized for the nanoconfined

synthesis of the cathode phase. Similar to the anode phase, electrical conductivity and lithium redox activity are a prerequisite for this second electrode nano-network. Additionally, the synthesis pathway has to be compatible with the already present carbon anode and polymer electrolyte. The PPO-coated GDMC monoliths were infiltrated with a bifunctional sulfur-polymer composite, completing the 3-D interpenetrating EES nanostructure (Fig. 1a). Sulfur was chosen as the redox-active functional material. It exhibits a discharge voltage of 2-2.5 V versus lithium and is efficiently infiltrated into pores down to the microporous regime (<2 nm) using liquid/vapor infiltration at moderate temperatures (155 °C).43 This made sulfur a preferred cathode material for our solid-state interpenetrating 3-D gyroidal hybrids over commonly employed oxides such as lithium cobalt oxide (LCO). Synthesis conditions of LCO necessitate high temperatures to obtain the required crystal structure. 44 The presence of thin polymer electrolyte (PPO) layers excluded these or other aggressive conditions. Additionally, many lithium metal oxides exhibit high lithiation potentials (>3.8 V vs. Li/Li⁺), exceeding the limit of our polymer electrolyte.41 The electronically conducting polymer poly-(3,4-ethylenedioxythiophene) (PEDOT) was included in the cathode network as an integrated nanostructured current collector, since sulfur is electronically insulating. PEDOT is commonly applied using aqueous polymer dispersions, which are inefficient for nanopore infiltration. Therefore, we utilized an in situ infiltration-polymerization method. To this end, the monomer, EDOT, and the oxidizing reagent, iron(III) para-toluenesulfonate, were infiltrated as small molecular entities enabling nanoconfined PEDOT synthesis within the remaining PPO-coated and sulfur infiltrated mesopore network of the GDMCs. In contrast to the anode side, the composite cathode network was thus constructed from two distinct materials acting as redox-active component (sulfur) and current collector (PEDOT), respectively.

We separately tested the conductivity of the 3-D integrated nanostructured PEDOT current collector prepared by this method. To this end, we independently synthesized insulating double gyroidal mesoporous polymer (G^DMP) monoliths by limiting the heat treatment of self-assembled ISO-resol hybrids to 450 °C (see the ESI†). These insulating G^DMP monoliths have otherwise identical structural features to G^DMC s and were used to test the percolation and conductivity of PEDOT chemically synthesized within the nanoscopic confinement of the gyroidal mesopore network. Resistance across the G^DMP monoliths measured before and after PEDOT polymerization decreased substantially (Fig. 3a), suggesting successful percolation of conductive PEDOT through the insulating polymer framework.

Comprehensive SEM and energy dispersive X-ray spectroscopy (EDS) analysis suggested that infiltration of sulfur and PEDOT into the mesopores of PPO coated G^DMC monoliths was fairly homogeneous (Fig. 3b, c and Fig. S4b–d, ESI†). With the measured carbon-to-sulfur weight ratio of three and assuming the PPO shell volume to be equal to the carbon matrix volume (density of PPO: 1.06 g cm⁻³), the estimated maximum areal sulfur loading was 2.4 mg cm⁻². This sulfur loading yielded a theoretical areal cathode capacity of 4 mA h cm⁻² (1675 mA h g⁻¹ of sulfur). PEDOT overlayers of a few microns on either surface of the

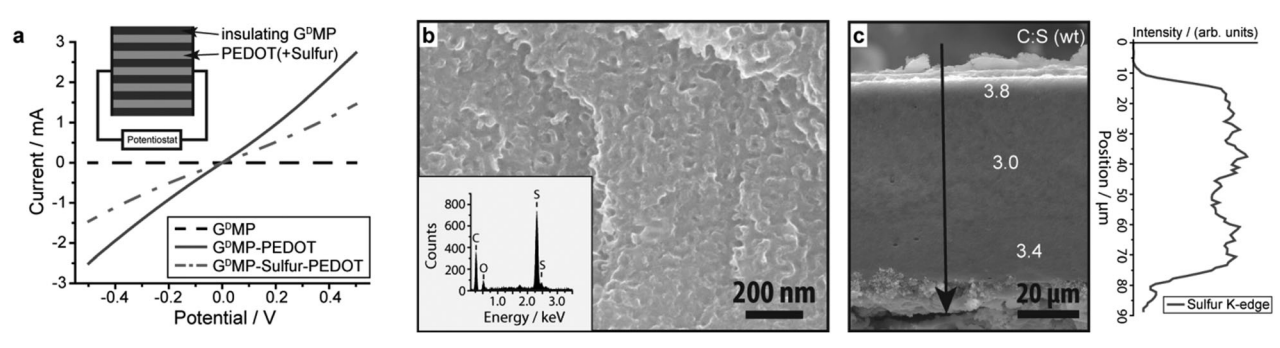


Fig. 3 Cathode composite infiltration. (a) Two-electrode resistance measurements through insulating double gyroidal mesoporous polymer monoliths (GDMP, dashed black), back-filled with PEDOT (solid grey), and sulfur-PEDOT composite (dash-dotted grey). Inset: Schematic representation of resistance measurement. (b and c) Cross-sectional SEM images of a sulfur-PEDOT backfilled PPO-coated G^DMC at high (b) and low (c) magnification with the corresponding EDS spectrum (b) and EDS line scan (c) of the sulfur K-edge signal across the film (line scan position indicated by an arrow in SEM and shown in Fig. S4b, ESI†). Numbers in (c) are the corresponding EDS-derived carbon: sulfur weight ratios at the respective positions.

monoliths could be readily distinguished after PEDOT infiltration (Fig. 3c). However, the outer monolith surfaces still exhibited gyroidal features after only sulfur infiltration (Fig. S4a, ESI†), indicating minimal levels of external sulfur. The PEDOT overlayers were used for subsequent electrical contacting of the cathode composite phase (Fig. 4a).

At this point, the step-wise and bottom-up synthesized gyroidal nanohybrids contained all the necessary EES components fully integrated on the nanoscale in 3-D, but both electrodes were present unlithiated and in their oxidized state. To introduce lithium, the sulfur-PEDOT phase was electrochemically reduced using lithium metal as the counter electrode in a two-electrode configuration (Fig. 4b). The discharge curve exhibited two plateaus at around 2.4 V and 1.4 V vs. Li/Li⁺, respectively (Fig. 4b). The first plateau at 2.4 V with a capacity of approximately 1 mA h cm⁻² matched well with the sulfur reduction potential and the capacity estimated above to form long-chain polysulfides, while the second plateau at 1.4 V was over 500 mV below the commonly observed one. 43,45 The large overpotential of the second plateau was anticipated, however, as PEDOT becomes insulating at these low potentials, 46 adding ohmic resistance. The shuttling of polysulfide species is a common problem in lithium-sulfur batteries due to their high solubility in organic electrolytes, potentially causing leakage of polysulfides during this external reduction of the gyroidal sulfur phase to lithium sulfide. Since polysulfides show strong absorption in the visible region, but no such discoloration was observed in the electrolyte solutions during this step, we can safely exclude that excessive leakage took place. 45

Electrochemical properties

Our bottom-up synthesis concept of a fully 3-D nano-integrated EES system yielded a gyroidal nanohybrid consisting of a carbon anode network conformally coated with an electronically insulating and ionically conducting polymer solid state electrolyte (PPO) that in turn is infiltrated with a bifunctional cathode composite of lithium sulfide and PEDOT (Fig. 1a). The cathode and anode phases were individually contacted during the process, making them accessible for electrochemical characterization. The gyroidal nanohybrid monoliths exhibited a stable open-circuit voltage at around 2.8 V (Fig. 4c) after being charged to 3.5 V. The high charging potential and lower open-circuit voltage after charging were assumed to originate from large polarization and leakage

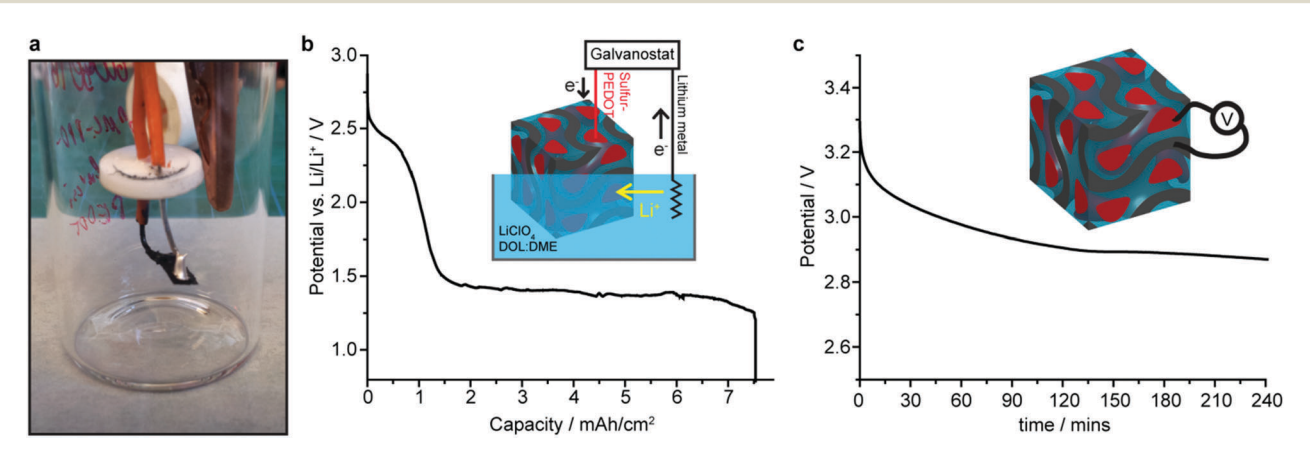


Fig. 4 Lithiation of the multifunctional 3-D gyroidal nanohybrids. (a) Photograph of a fully assembled tetrafunctional gyroidal nanohybrid device before external lithiation. (b) Potential during external lithiation of the gyroidal sulfur-PEDOT phase vs. lithium metal in liquid electrolyte at a current of 0.125 mA cm⁻². (c) Open circuit voltage of the solid-state gyroidal hybrid over the first 4 hours after charge.

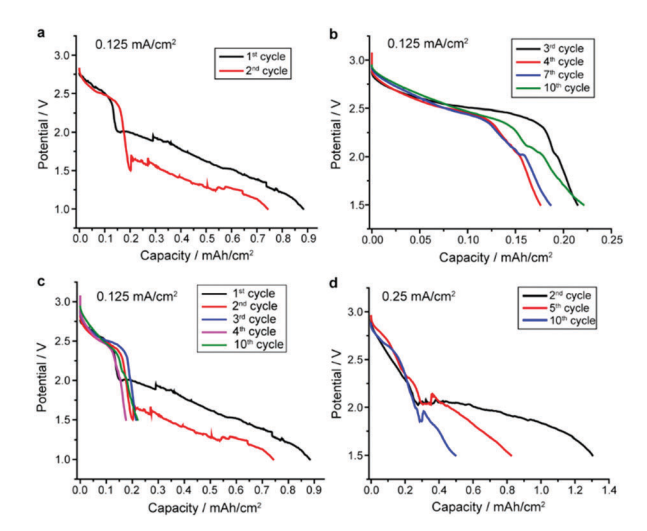


Fig. 5 Electrochemical characterization of the solid-state 3-D gyroidal nanohybrids. (a-c) Discharge curves of a gyroidal nanohybrid EES at a current of 0.125 mA cm⁻²: (a) first two cycles with the lower cut-off potential at 1 V. (b) Selected subsequent cycles with the lower cut-off potential at 1.5 V. (c) Overlay of selected cycles at 0.125 mA cm⁻². (d) Discharge curves of selected cycles of a gyroidal nanohybrid EES at a current of 0.25 mA ${\rm cm}^{-2}$ with the lower cut-off potential at 1.5 V.

currents through the electrolyte layer at potentials above 3 V. Welldefined discharge plateaus were observed upon galvanostatic cycling the 3-D nano-interpenetrating anode and cathode phases as an EES (Fig. 5 and Fig. S5, ESI†). When discharged to 1 V at a current density of 0.125 mA cm⁻², the discharge curves exhibited a reversible plateau at around 2.7 V with a capacity of up to 0.18 mA h cm⁻² and further irreversible capacity at lower potentials with a maximum capacity of 0.9 mA h cm⁻² (Fig. 5a). The reversibility of the first discharge plateau was confirmed by stable cycling up to ten times with a lower voltage cut-off at 1.5 V (Fig. 5b and c) with reversible capacities of around 0.2 mA h cm⁻². Cycling of the solid-state gyroidal nanohybrid EES at twice the rate (0.25 mA h cm⁻²) for another 10 cycles, also yielded the reversible discharge plateau above 2.5 V with the same discharge capacities of around 0.2 mA cm⁻², and irreversible discharge below 2.1 V (Fig. 5d). The irreversibility at lower potentials was assumed to originate from the conductor-insulator transition of PEDOT. The measured reversible capacity correlates to approximately 16 mA h g⁻¹ on the device scale, taking into account the mass of all 3-D integrated components (anode, electrolyte, cathode and integrated current collector), 45 times higher than that of the only previously reported solid-state 3-D prototype with nanoscale dimensions.²⁸ Other microbatteries using 3-D architectures with higher capacities have been reported, however, using designs with micronscale electrode separation and liquid electrolytes.^{24,26}

The sulfur loading in the present architecture would allow for capacity matching of the carbon anode with the first discharge plateau of sulfur that lies within the conductivity window of PEDOT with an overall theoretical capacity of 1 mA h cm⁻². This capacity matching and utilization of only the first sulfur discharge plateau has the advantage of minimal volume expansion of the cathode as compared to full lithiation

of sulfur. The achieved reversible capacity displayed by our gyroidal nanohybrid EES is approximately 20% of its theoretical capacity, but it clearly arises from accessing material throughout the 3-D monoliths, since there is no appreciable amount of sulfur on the top or bottom surfaces of the monoliths (vide supra). Similarly, based on the mass of sulfur, the maximum specific capacity obtained is 375 mA h g⁻¹, 22% of its theoretical capacity. These results suggest the formation of electronically disconnected parts of the nano-integrated cathode phase from the external current collector after, or the dissolution of polysulfide species during, external lithiation. The volume change of sulfur during full lithiation and delithiation, especially during the initial external lithiation, potentially caused the conductive PEDOT network to lose connectivity to parts of the gyroidal cathode network. Despite its inefficiencies though, our results clearly establish the proof-of-concept and feasibility of a self-assembly derived nanoscale 3-D interpenetrating cathode and anode architecture for electrical energy storage. This is particularly noteworthy in light of the fact that a solid-state separator only 10 nm in thickness, covering a large absolute area of approximately 400 cm² throughout a tortuous macroscopic monolithic device, was able to maintain an open circuit voltage of over 2.8 V for hours and a well-defined discharge plateau for up to 20 cycles. Our results suggest that after all processing steps and despite its small thickness, the polymer electrolyte is sufficiently pinhole-free and impermeable to the sulfur-PEDOT cathode phase over this entire area to prevent short circuits. While at first this appears surprising, it is perhaps instructive to remember that biology uses selfassembly of lipids to maintain a potential difference of around 0.1 V across even thinner liquid-state cell membranes throughout the entire body.47

Conclusions

We have demonstrated the bottom-up synthesis of a macroscopic nano-3-D interpenetrating solid-state electrochemical energy storage device architecture with precise spatial control over four distinct functional materials with individual domain dimensions of 20 nm or less. The 3-D architecture allows for a substantial decrease in footprint area, due to folding and integration of all nanoscaled electrochemical components into interpenetrating networks, and by exploiting the third dimension. Thus, it represents a truly atom-efficient approach. Our co-continuous nanohybrids consist of two interpenetrating redox-active cathode/current collector composite nanonetworks (sulfur/PEDOT) separated from a carbon anode matrix by an ultrathin, pinhole-free polymer electrolyte layer (PPO) that is wrapped around the interpenetrating gyroidal electrodes. The synthesis concept allowed separate electric contacting of the carbon and sulfur nano-interpenetrating electrode networks. The resulting nano-3-D EES maintained a stable open-circuit voltage and a well-defined discharge plateau at 2.7 V with a reversible capacity of $0.2 \text{ mA} \text{ h cm}^{-2}$. As an illustrative comparison, keeping layer dimensions and materials the same, a flat,

three-layer (anode, separator and cathode) battery design, with comparable capacity, would take up an area that would be 4700 times larger. In other words, a planar thin film battery with the same critical dimension would have a maximum theoretical capacity of 2.7×10^{-4} mA h cm⁻². Even at only 20% utilization of the theoretical maximum capacity of the device demonstrated here, this would still account for an area of about 940 times larger.

While these proof-of-principle results of 3-D gyroidal electrochemical energy storage devices are stimulating and promising, continued work is required to carefully assess how improved materials, processes, and housing can lead to enhanced performance. For example, the glass-vial set-up employed here for housing the 3-D nanohybrid energy storage device (Fig. 4a) was not optimized in any way and likely led to air contamination and subsequent failure of the device during the storage period after the 20 cycles described here. Other limitations in the device presented here are the relatively low coulombic efficiency, non-quantitative utilization of the cathode material, and poor conductivity of the cathode current collector at low potentials. Some of these drawbacks may be overcome with alterations to the cathode composite, such as widening the conductivity window, or combining redox activity and current collector in one material. The exploration, synthesis, and integration of such materials into nano-3-D battery designs as described here provides fuel for an exciting future in this field of research, as our work demonstrates that such devices are feasible and their further development worth pursuing. In particular, implementation of different functional materials in our nano-3-D battery concept requires adjustment of the synthetic procedures, since the electrolyte and the 2nd electrode are synthesized successively within the 1st electrode. This aspect makes their fabrication fundamentally different from classic battery research, in which the individual components are fabricated separately and then physically assembled in a stack, requiring no compatibility of their individual syntheses. Materials that could potentially be implemented with only limited synthetic alterations are block copolymer derived mesoporous metal oxide-carbon hybrids as anode materials, and redox-active and conductive polymers as infiltrated cathode materials.48-52

It is important to emphasize that at this early stage of research into the synthesis of such multifunctional nano-3-D interpenetrating EES architectures, it is not realistic to expect the resulting monolithic devices to exhibit optimal electrochemical performance. Indeed, to the best of our knowledge, no reports exist to date on the synthesis of such complex co-continuous 3-D gyroidal device nano-architectures described herein. Instead, our intent was to establish a "proof-ofprinciple" for overcoming a number of the existing hurdles and answering critical questions. For example, could chemical pathways generate interpenetrating nanonetworks of all phases with the right connectivity and separation that serve the functions of all battery components? And would it be possible to observe a stable potential across the fully assembled monolithic nano-3-D EES device, potentially even with a few reversible

charge/discharge cycles in which lithium ions travel only tens of nanometers while electrons travel over macroscopic dimensions through an external electrical circuit to provide electrical energy? In this report, we demonstrated that such complex co-continuous, multifunctional, and interpenetrating gyroidal solid-state hybrid architectures can be successfully synthesized and that they indeed display a battery-like redox behavior and charge/discharge profiles with stable open circuit voltage, thereby demonstrating a plausible path to solid-state nano-3-D batteries. Additionally, all components of our synthesis concept were chosen to be mutually compatible with facile laboratory processing. They are either polymer chemistry based (polymer self-assembly based anode formation; electropolymerization of solid electrolyte; solution polymerization of cathode current collector) or moderate temperature processable (active cathode material). In particular, the synthesis does not include any expensive or time-consuming top-down 3-D nanofabrication, making the approach accessible to a wide community. We hope that this work will spur interest in further development and improvement of multifunctional, fully integrated 3-D nanohybrid architectures for electrical energy storage.

Experimental

Gyroidal mesoporous carbon (GDMC)

The G^DMC monoliths were synthesized using block copolymer (BCP) self-assembly. The structure directing amphiphilic triblock terpolymer poly(isoprene)-block-poly(styrene)-block-poly-(ethylene oxide) (ISO) was synthesized via a step-wise anionic polymerization.⁵³ The characteristics of the ISO are summarized in Table S1 (ESI†). Phenol-formaldehyde resols were used as carbon precursors and synthesized using oligomerization of phenol and formaldehyde in a molar ratio of 1:2 under basic conditions. 40 Monolithic ISO:resol hybrids with double gyroidal (GD) morphology were obtained by dissolution of both components in a 1:0.54 weight ratio in tetrahydrofuran and chloroform (1:1 by weight), followed by solvent evaporation and annealing. The polymer-organic hybrid monoliths were plasma treated to remove surface capping layers before carbonization under inert gas flow above 1000 °C. Free-standing GDMC monoliths were cut into rectangular shapes with footprint areas of 0.08-0.14 cm², attached to a wire in an edge-on geometry with silver epoxy (EPO-TEK H20E from EMS), and the contact was sealed with silicone rubber (Momentive RTV 108). Insulating gyroidal mesoporous polymer (GDMP) materials were obtained from the same ISO-resol hybrids as G^DMCs, but were subjected to heat treatment at only 450 °C under nitrogen for 3 hours yielding insulating phenolic resins.54

Electrodeposition of polymer electrolyte

The walls and surfaces of the conductive and redox-active G^DMC electrodes were conformally coated with poly(phenylene oxide) (PPO) using self-limiting electropolymerization. The polymerization solution in acetonitrile was 0.05 M in phenol and tetramethylammonium hydroxide pentahydrate, and 0.1 M in

tetrabutylammonium perchlorate (TBAP). Electropolymerization was conducted in a three-electrode set up with a platinum counter electrode and a Ag/Ag $^{+}$ reference electrode (silver wire in acetonitrile with 0.05 M silver perchlorate and 0.1 M TBAP) under an inert atmosphere using a Metrohm Autolab PGSTAT204 potentiostat. Phenol was oxidatively polymerized using pulsed potentiostatic deposition with 200 pulses at +0.6 V vs. Ag/Ag $^{+}$ for a duration of 5 s with a 10 s equilibration between each pulse. 42 Pulsed polymer electrodeposition was followed by cyclic voltammetric sweeps between -0.4 V and +0.6 V vs. Ag/Ag $^{+}$ at 20 mV s $^{-1}$. The mesoporous PPO-coated carbon monoliths were subsequently cleaned with ethanol and dried at room temperature in air.

Sulfur infiltration

Sulfur, employed as the cathode material, was introduced into the mesopores of PPO-coated G^DMCs through liquid/vapor infiltration at 155 $^{\circ}C$ for 24 hours. To this end, excess sulfur powder (1–3 mg) was put on and around the monoliths (with footprint area of 0.08–0.14 cm², see above) in a sealed glass container, and heated at 155 $^{\circ}C$ for 24 hours.

Integrated polymeric current collector infiltration

Poly(ethylenedioxythiophene) (PEDOT) was chemically polymerized inside the PPO-coated and sulfur infiltrated G^DMC monolith mesopores using oxidative polymerization. A 0.7 M iron(III) *para*-toluenesulfonate solution in ethanol was freshly prepared and EDOT was added to make a 1 M EDOT solution. The G^DMC-PPO-sulfur monoliths were immersed in the solution for 20 min at 4 °C. The monolith was removed from the polymerization solution without further treatment and the 3-D nanohybrid was subsequently dried in air at room temperature and 80 °C. The sulfur-PEDOT nanostructured composite phase was then contacted with silver epoxy and sealed with silicone rubber.

Sulfur lithiation and galvanostatic testing

The content of carbon and sulfur in the fully assembled gyroidal nanohybrids was approximately 5 mg cm $^{-2}$ and 2.4 mg cm $^{-2}$, respectively. The contacted tetrafunctional monolithic nanohybrid was immersed horizontally (*i.e.* parallel to the gas–liquid interface) in 1 M lithium perchlorate in a mixture of dioxolane (DOL) and dimethoxyethane (DME) (1:1 by volume) together with lithium foil in a septum capped vial under an argon atmosphere. The sulfur–PEDOT phase was discharged to 1 V νs . Li/Li $^{+}$ at a current of 0.125 mA cm $^{-2}$. After lithiation of the sulfur–PEDOT nanocomposite, the lithium foil was disconnected, and the penta-continuous and tetrafunctional nanohybrids were cycled with the nanostructured $G^{\rm D}MC$ and sulfur–PEDOT phases connected as anode and cathode, respectively, with varying cut-off voltages as described in the text after removal of the liquid electrolyte.

Characterization

Scanning electron microscopy (SEM) analysis of carbonized samples was carried out using a Zeiss LEO 1550 FE-SEM or a Tescan Mira SEM operating at an accelerating voltage of 10–20 kV. The SEM was equipped with a Bruker energy dispersive spectrometer (EDS) for elemental analysis. SAXS measurements

were performed on the monolithic parent hybrid and the resulting carbon materials at the Cornell High Energy Synchrotron Source (CHESS). Nitrogen sorption isotherms were obtained using a Micromeritics ASAP 2020 surface area and porosity analyzer at -196 °C. Lithiation and galvanostatic tests of monolithic carbon materials and tetrafunctional nanohybrids were executed using a BST8-WA 8-channel battery analyzer obtained from MTI Corporation. Resistance through the PPO thin film of the PPO-coated G^DMC monoliths and of the PEDOT and sulfur-PEDOT infiltrated insulating gyroidal mesoporous polymer (GDMP) frameworks was measured using cyclic voltammetry at a scan rate of 50 mV s⁻¹ with an AUTOLAB Metrohm Autolab PGSTAT204. The second contact for the uncoated and PPO-coated carbon monoliths was made using a liquid gallium-indium eutectic contact on one of the surfaces. Contacts for the PEDOT and sulfur-PEDOT infiltrated insulating GDMP framework were made with silver epoxy (EPO-TEK H20E from EMS) on both surfaces.

Conflicts of interest

The authors declare no competing financial interests. A patent application related to this research has been filed by Cornell University.

Acknowledgements

We thank Dr J. Gao for assistance with the coin cell test and Dr Kate Barteau for helpful discussions. This work was primarily supported as part of the Energy Materials Center at Cornell (emc²), an Energy Frontier Research Center funded by the U.S. Department of Energy, Office of Science, Basic Energy Sciences under award no. DE SC0001086. This work made use of the Cornell Center for Materials Research Shared Facilities supported through the NSF MRSEC program (DMR-1719875). This work was further based upon research conducted at the Cornell High Energy Synchrotron Source (CHESS) supported by the National Science Foundation and the National Institutes of Health/National Institute of General Medical Sciences under NSF award no. DMR-1332208. J. G. W. acknowledges partial support from the National Science Foundation (NSF) under award no. DMR-1707836.

References

- 1 A. D. Franklin, Science, 2015, 349, aab2750.
- 2 S. E. Thompson and S. Parthasarathy, *Mater. Today*, 2006, 9, 20–25.
- 3 T. Ito and S. Okazaki, Nature, 2000, 406, 1027-1031.
- 4 C. R. K. Marrian and D. M. Tennant, *J. Vac. Sci. Technol.*, *A*, 2003, 21, S207–S215.
- 5 A. W. Topol, D. C. La Tulipe, L. Shi, D. J. Frank, K. Bernstein, S. E. Steen, A. Kumar, G. U. Singco, A. M. Young, K. W. Guarini and M. Ieong, *IBM J. Res. Dev.*, 2006, 50, 491–506.

- 6 A. Llordés, G. Garcia, J. Gazquez and D. J. Milliron, Nature, 2013, 500, 323-326.
- 7 S. H. Joo, S. J. Choi, I. Oh, J. Kwak, Z. Liu, O. Terasaki and R. Ryoo, Nature, 2001, 412, 169-172.
- 8 A. Yella, H.-W. Lee, H. N. Tsao, C. Yi, A. K. Chandiran, M. K. Nazeeruddin, E. W.-G. Diau, C.-Y. Yeh, S. M. Zakeeruddin and M. Grätzel, Science, 2011, 334, 629-634.
- 9 H.-B. Sun and S. Kawata, Adv. Polym. Sci., 2006, 170, 169–273.
- 10 G. M. Whitesides and B. Grzybowski, Science, 2002, 295, 2418-2421.
- 11 M. C. Orilall and U. Wiesner, Chem. Soc. Rev., 2011, 40, 520-535.
- 12 D. R. Rolison, J. W. Long, J. C. Lytle, A. E. Fischer, C. P. Rhodes, T. M. McEvoy, M. E. Bourg and A. M. Lubers, Chem. Soc. Rev., 2009, 38, 226-252.
- 13 J. W. Long, B. Dunn, D. R. Rolison and H. S. White, Chem. Rev., 2004, 104, 4463-4492.
- 14 J. M. Tarascon and M. Armand, Nature, 2001, 414, 359-367.
- 15 Y. Gogotsi and P. Simon, Science, 2011, 334, 917-918.
- 16 A. S. Aricò, P. Bruce, B. Scrosati, J.-M. Tarascon and W. van Schalkwijk, Nat. Mater., 2005, 4, 366-377.
- 17 P. Simon, Y. Gogotsi and B. Dunn, Science, 2014, 343, 1210-1211.
- 18 J. R. Miller and P. Simon, Science, 2008, 321, 651-652.
- 19 P. G. Bruce, B. Scrosati and J.-M. Tarascon, Angew. Chem., Int. Ed., 2008, 47, 2930-2946.
- 20 Y. Sun, N. Liu and Y. Cui, Nat. Energy, 2016, 1, 16071.
- 21 K. G. Gallagher, S. E. Trask, C. Bauer, T. Woehrle, S. F. Lux, M. Tschech, P. Lamp, B. J. Polzin, S. Ha, B. Long, Q. Wu, W. Lu, D. W. Dees and A. N. Jansen, J. Electrochem. Soc., 2016, 163, A138-A149.
- 22 H. Sun, L. Mei, J. Liang, Z. Zhao, C. Lee, H. Fei, M. Ding, J. Lau, M. Li, C. Wang, X. Xu, G. Hao, B. Papandrea, I. Shakir, B. Dunn, Y. Huang and X. Duan, Science, 2017, 356, 599-604.
- 23 N. J. Dudney, Mater. Sci. Eng., B, 2005, 116, 245-249.
- 24 J. H. Pikul, H. Gang Zhang, J. Cho, P. V. Braun and W. P. King, Nat. Commun., 2013, 4, 1732.
- 25 M. Roberts, P. Johns, J. Owen, D. Brandell, K. Edstrom, G. El Enany, C. Guery, D. Golodnitsky, M. Lacey, C. Lecoeur, H. Mazor, E. Peled, E. Perre, M. M. Shaijumon, P. Simon and P.-L. Taberna, J. Mater. Chem., 2011, 21, 9876.
- 26 K. Sun, T. S. Wei, B. Y. Ahn, J. Y. Seo, S. J. Dillon and J. A. Lewis, Adv. Mater., 2013, 25, 4539-4543.
- 27 H.-S. Min, B. Y. Park, L. Taherabadi, C. Wang, Y. Yeh, R. Zaouk, M. J. Madou and B. Dunn, J. Power Sources, 2008, 178, 795-800.
- 28 N. S. Ergang, M. A. Fierke, Z. Wang, W. H. Smyrl and A. Stein, J. Electrochem. Soc., 2007, 154, A1135.
- 29 C. P. Rhodes, J. W. Long, K. A. Pettigrew, R. M. Stroud and D. R. Rolison, Nanoscale, 2011, 3, 1731-1740.
- 30 J. G. Werner, M. R. J. Scherer, U. U. Steiner and U. Wiesner, Nanoscale, 2014, 6, 8736-8742.
- 31 T. H. Epps, E. W. Cochran, T. S. Bailey, R. S. Waletzko, C. M. Hardy and F. S. Bates, Macromolecules, 2004, 37, 8325-8341.

- 32 D. A. Hajduk, P. E. Harper, S. M. Gruner, C. C. Honeker, G. Kim, E. L. Thomas and L. J. Fetters, Macromolecules, 1994, 27, 4063-4075.
- 33 B. D. Wilts, B. Apeleo Zubiri, M. A. Klatt, B. Butz, M. G. Fischer, S. T. Kelly, E. Spiecker, U. Steiner and G. E. Schröder-Turk, Sci. Adv., 2017, 3, e1603119.
- 34 G. E. Schröder-Turk, S. Wickham, H. Averdunk, F. Brink, J. D. Fitz Gerald, L. Poladian, M. C. J. Large and S. T. Hyde, J. Struct. Biol., 2011, 174, 290-295.
- 35 V. Luzzati and P. A. Spegt, Nature, 1967, 215, 701-704.
- 36 A. Schoen, NASA Tech. Note, 1970, D-5541.
- 37 F. S. Bates and G. H. Fredrickson, Phys. Today, 1999, 52, 32-38.
- 38 B.-K. Cho, A. Jain, S. M. Gruner and U. Wiesner, Science, 2004, 305, 1598-1601.
- 39 E. J. W. Crossland, M. Kamperman, M. Nedelcu, C. Ducati, U. Wiesner, D.-M. M.-M. Smilgies, G. E. S. Toombes, M. A. Hillmyer, S. Ludwigs, U. Steiner and H. J. Snaith, Nano Lett., 2009, 9, 2807-2812.
- 40 J. G. Werner, T. N. Hoheisel and U. Wiesner, ACS Nano, 2014, 8, 731–743.
- 41 C. P. Rhodes, J. W. Long, M. S. Doescher, J. J. Fontanella and D. R. Rolison, J. Phys. Chem. B, 2004, 108, 13079-13087.
- 42 R. L. McCarley, E. a. Irene and R. W. Murray, J. Phys. Chem., 1991, 95, 2492-2498.
- 43 X. Ji, K. T. Lee and L. F. Nazar, Nat. Mater., 2009, 8, 500-506.
- 44 X. Li, F. Cheng, B. Guo and J. Chen, J. Phys. Chem. B, 2005, **109**, 14017-14024.
- 45 M. Cuisinier, P.-E. Cabelguen, S. Evers, G. He, M. Kolbeck, A. Garsuch, T. Bolin, M. Balasubramanian and L. F. Nazar, J. Phys. Chem. Lett., 2013, 4, 3227-3232.
- 46 S. E. Burkhardt, G. G. Rodríguez-Calero, M. A. Lowe, Y. Kiya, R. G. Hennig and H. D. Abruña, J. Phys. Chem. C, 2010, 114, 16776-16784.
- 47 W. D. Stein and W. R. Lieb, Transport and diffusion across cell membranes, Academic Press, Orlando, Orlando, FLA., 1986.
- 48 J. Lee, M. C. Orilall, S. C. Warren, M. Kamperman, F. J. DiSalvo and U. Wiesner, Nat. Mater., 2008, 7, 222-228.
- 49 J. Lee, Y. S. Jung, S. C. Warren, M. Kamperman, S. M. Oh, F. J. DiSalvo and U. Wiesner, Macromol. Chem. Phys., 2011, 212, 383-390.
- 50 E. Kang, Y. S. Jung, G.-H. Kim, J. Chun, U. Wiesner, A. C. Dillon, J. K. Kim and J. Lee, Adv. Funct. Mater., 2011, 21, 4349-4357.
- 51 L. Shen, M. Mizutani, G. G. Rodríguez-Calero, K. Hernández-Burgos, T.-T. Truong, G. W. Coates and H. D. Abruña, J. Electrochem. Soc., 2017, 164, A1946-A1951.
- 52 G. G. Rodríguez-Calero, S. Conte, M. A. Lowe, J. Gao, Y. Kiya, J. C. Henderson and H. D. Abruña, Electrochim. Acta, 2015, 167, 55-60.
- 53 T. S. Bailey, C. M. Hardy, T. H. Epps and F. S. Bates, Macromolecules, 2002, 35, 7007-7017.
- 54 Y. Meng, D. Gu, F. Zhang, Y. Shi, L. Cheng, D. Feng, Z. Wu, Z. Chen, Y. Wan, A. Stein and D. Zhao, Chem. Mater., 2006, 18, 4447-4464.
- 55 K. H. Hong, K. W. Oh and T. J. Kang, J. Appl. Polym. Sci., 2005, 97, 1326-1332.